

# Transient Dynamics of Edge Flames in a Laminar Nonpremixed Hydrogen-Air Counterflow

Chun Sang Yoo and Hong G. Im

Department of Mechanical Engineering

University of Michigan, Ann Arbor, MI 48109-2125, USA

Corresponding author:

Prof. Hong G. Im  
Department of Mechanical Engineering  
University of Michigan  
2250 G.G. Brown Bldg.  
2350 Hayward St.  
Ann Arbor, MI 48109-2125, USA

Phone : (734) 615-5152  
Fax : (734) 647-3170  
Email : [hgim@umich.edu](mailto:hgim@umich.edu)

Word Count

Text : 3200 (from word processor)  
Equations : 70 (3 equations  $\times$  23words)  
References : 390 ( (20 references +2)  $\times$  2.3  $\times$  7.6)  
Figures : 1540 (7 figures  $\times$  160words + 1 figure  $\times$  180words + 1 figure  $\times$  240words)  
Tables : 130 (17 lines  $\times$  7.6 words)  
**Total : 5330**

Short Title:

Edge Flames in a Counterflow

Keywords:

Edge flame, extinction, flame speed, transient dynamics

Preferred Presentation :

Oral

Preferred Colloquium Topic Area :

Laminar Flames

Submitted to the 30<sup>th</sup> Symposium (International) on Combustion

University of Illinois at Chicago, Chicago, Illinois, USA, July 25-30, 2004.

# **Transient Dynamics of Edge Flames in a Laminar Nonpremixed Hydrogen-Air Counterflow**

Chun Sang Yoo and Hong G. Im  
Department of Mechanical Engineering  
University of Michigan  
Ann Arbor, MI 48109-2125, USA

## **Abstract**

Dynamics of edge flames encountered upon local quenching of nonpremixed flames is studied numerically considering detailed chemistry of hydrogen-air combustion. The simulations are performed by superimposing two pairs of counter-rotating vortices on a steady counterflow nonpremixed flame. The density-weighted displacement speed and scalar dissipation rate are found to be appropriate parameters in characterizing the propagation speed of the edge flame with finite thickness and chemical structure, for both steady and transient conditions. It is also found that the edge flame speed depends strongly on the transient and history effects of the imposed flow field in addition to the instantaneous local scalar dissipation rate. A negative edge flame speed is observed during the early phase of the interaction due to the enthalpy loss to the transverse direction in the presence of a large strain. The effects of the fuel Lewis number on the edge flame speed are found to be consistent with the previous theoretical predictions based on the laminar flamelet theory. The results suggest that the transient and history aspects need to be carefully taken into account for an accurate description of the realistic turbulent nonpremixed combustion with partial quenching.

## Introduction

The local quenching of counterflow nonpremixed flames and subsequent edge flame formation have widely been investigated to gain fundamental understanding of turbulent nonpremixed combustion, where the flames are subjected to partial extinction and re-ignition in the presence of strong turbulence [1-3]. It is believed that the dynamics of the edge flame response to the neighboring flow conditions is the key stabilization mechanism for the lifted diffusion flame [4,5]. Furthermore, the leakage of unburned reactants through the quenched opening can contribute significantly to the pollutant formation such as carbon monoxide or unburned hydrocarbon. Therefore, to develop a predictive model that can accurately describe highly-turbulent combustion, it is important to characterize the edge propagation behavior as a function of relevant physical parameters.

Depending on the propagation speed relative to the upstream reactant flow, the edge flames are classified into two types, namely the ignition front (recovering the quenched hole) and the failure wave (extending the hole leading to a total extinction) [6]. It has been found that the most important physical parameters dictating the edge propagation behavior are the scalar dissipation rate, which represents the rate of mixing ahead of the flame edge, and the reactant Lewis number characterizing the unequal rate of mixing. A theoretical study employing simple chemistry [7] predicted that the edge speed can assume positive or negative values near the diffusion flame extinction condition depending on the Lewis number. Qualitatively consistent results have been observed in a numerical study with one-step chemistry [8]. Additional effects of volumetric heat loss on the edge propagation speed have also been studied [9].

While such a well-defined steady problem can provide clear baseline information about the edge flame behavior, in real turbulent combustion the edge dynamics are much more

complicated as a result of heat release, detailed flame structure, and strong flow transients. Furthermore, correlation of the edge propagation with the uniform scalar dissipation rate based on the system configuration and its direct application to turbulent combustion submodels is questionable, because such a well-defined global parameter in the neighborhood of the edge flame is very difficult to identify in realistic turbulent reacting flows. In all likelihood, the correlation has to be determined based on the local parameters, which may lead to large uncertainties in quantitative evaluation of the important observables.

To investigate the edge responses in more realistic situations, numerical simulations of the nonpremixed edge flames have been performed as a flame-vortex interaction with simple chemistry [10,11], in a counterflow configuration with hydrogen-air chemistry [12,13], as a steady propagation with methanol-air chemistry [14], and as a transient ignition front dynamics with hydrogen-air chemistry [15,16]. Throughout these detailed simulation studies, consideration of the realistic effects resulted in difficulties in unique determination of the edge flame speed in terms of a few simple physical parameters. In particular, in contrast to the theoretical prediction [7], the existence of negative edge flame speed was hardly found in direct simulation studies, with a few exceptions [15,16] in which a negative flame speed was observed during the phase of intense interaction with the flame edge and counter-rotating vortices. Furthermore, the effects of flow transients leading to a wide variation in the edge flame dynamics have been noted [10-13,15,16].

Therefore, the main objectives of this paper are (a) to investigate the issues related to the ambiguities in the definition of the edge flame speed, (b) to assess the effect of Lewis number and (c) to analyze the impact of flow transients on the edge flame dynamics. High-fidelity simulations of a counterflow hydrogen-air system with detailed chemistry and variable Lewis

number are performed where edge flames are generated by prescribed vortex pairs impinging onto each other. The configuration serves as a canonical setting to allow a systematic investigation of the various parameters, thereby providing insight towards understanding of the realistic turbulent nonpremixed edge flame characteristics.

## Numerical Configuration

Figure 1 shows the schematic of the computational configuration under study. The computational domain is 5.0mm×5.0mm with 500 grid points in each direction. A steady counterflow diffusion flame is established by specifying the potential flow conditions at both fuel and oxidizer inlet boundaries. The fuel stream is hydrogen diluted with 50% nitrogen by volume, and the oxidizer stream is air. The temperature of both streams is at 300K, and the pressure is 1 atm. A compressible reacting flow code with a 4th order Runge-Kutta time integration and an 8th order central differencing schemes [16] is used. A detailed hydrogen-air kinetic mechanism [17] is adopted, and a temperature dependent viscosity and constant Lewis numbers determined at 1000K are used for individual species. The constant Lewis number approximation in fact works favorably in the present study since it allows an arbitrary adjustment of the fuel Lewis number for a parametric investigation. To achieve a stable counterflow flames, the soft-inflow boundary conditions [18] are used at both inlet boundaries and the nonreflecting conditions are used at both exit boundaries. The domain size and duration of computation are carefully monitored to ensure that the results are not affected by the boundary conditions.

Two pairs of counter-rotating vortices are superimposed as [15]:

$$\frac{u_{\theta}(r)}{u_{\theta,\max}} = \frac{0.9833\sigma^2}{2\pi r^2 [1 - e^{-(r/\sigma)^3}]} \quad (1)$$

where  $\sigma$  is the effective radius such that the maximum azimuthal velocity,  $u_{\theta, \max}$ , occurs at  $r = 0.9\sigma$ .

Five different cases of the initial vortex strength and Lewis numbers of hydrogen are studied as shown in Table 1. For all cases, the strain rate induced by the vortices is sufficiently strong to quench the laminar nonpremixed flame upon interaction, and the quenched flame segments are convected out of the computational domain by the mean tangential flow. Cases A through C are identical except the strength of the vortices, and in Cases D and E the Lewis number for hydrogen is artificially modified to study the effects of fuel diffusivity.

## Results and Discussion

### *Existence of Negative Displacement Speed*

Figure 2 shows the temporal evolution of heat release isocontours for Cases A to C. For all the cases, the two edges appear to move away from each other. As will be discussed later, however, this does not necessarily imply that the edges have a negative speed, but they can be merely blown out by the vortex-induced convective flow. It is also observed that, although the detailed structure of the edges depends on the initial vortex strength, the maximum heat release point appears to align with the stoichiometric mixture fraction line quite well.

Figure 3 shows the history of the heat release rate evaluated along the stoichiometric mixture fraction line, plotted versus the  $y$ -position for case A. The quantity is normalized by the maximum heat release rate of the “reference” premixed flame, which is based on the stoichiometric mixture of the fuel and oxidizer streams. When a counterflow nonpremixed flame interacts with the impinging vortices, the center of reaction zone is subjected to a large value of scalar dissipation rate,  $\chi$ . Initially, the heat release rate increases due to the increased mass flux

to the flame ( $t = 0.119\text{ms}$ ), almost up to that of the reference premixed flame, consistent with the simple-chemistry simulation results [10]. Subsequently, the local quenching of the flame occurs at the center of the flame due to excessive mass flux and heat, and two distinct edges are formed ( $t = 0.265\text{ms}$ ). The onset of edge flames is defined as the time at which the heat release rate between the two edges falls below 1% of the initial value, which corresponds to  $t = 0.265\text{ms}$  for Case A.

To analyze the local edge propagation speed, the density-weighted displacement speed,  $S_d^*$ , is defined as [15]

$$S_d^* \equiv \frac{\rho S_d}{\rho_u} = \frac{1}{\rho_u |\nabla Y_{\text{H}_2\text{O}}|} \left[ w_{\text{H}_2\text{O}} + \frac{\partial}{\partial x} \left( \rho D_{\text{H}_2\text{O}} \frac{\partial Y_{\text{H}_2\text{O}}}{\partial x} \right) + \frac{\partial}{\partial y} \left( \rho D_{\text{H}_2\text{O}} \frac{\partial Y_{\text{H}_2\text{O}}}{\partial y} \right) \right], \quad (2)$$

which is evaluated at the intersection between the isocontour of the water mass fraction and the stoichiometric mixture fraction line. The scalar dissipation rate,  $\chi = 2\alpha |\nabla \xi|^2$ , is also evaluated at the same location, where  $\xi$  is the mixture fraction following Bilger's formula [19], and  $\alpha = \lambda / \rho c_p$  is the local thermal diffusivity. As would be the case in real turbulent flames, it is difficult to define a global characteristic scalar dissipation rate for the present configuration, such that it is sensible to choose the local variables to describe the edge flame behavior.

Simulations of the flame-vortex interaction have revealed a significant amount of transient dynamics within the edge flame structure during the initial stage of the edge formation. Figure 4 shows the density-weighted displacement speed along the stoichiometric mixture fraction line,  $\xi = \xi_{\text{st}}$ , for Case A at the onset of the edge formation ( $t = 0.265\text{ms}$ ) and at a later time ( $t = 0.367\text{ms}$ ). While a steadily-propagating edge flame was found to exhibit only small variations in the displacement speed within the flame [15], in the present study the displacement speed varies widely from a negative to positive speed across the thermal thickness (shown in a shaded area) at

the onset of the edge formation (Fig. 4(a)). The large variation in the displacement speed implies that the edge flame thickness is being compressed due to the high scalar dissipation rate. At a later time, however, the edge flame speed has only positive values with much smaller variations throughout the thermal thickness (Fig. 4(b)), thereby recovering the steady edge flame characteristics.

To identify the main reason to cause the negative edge flame speed, the contributions of the individual terms in RHS of Eq. (2) to the displacement speed are examined. Figure 5 shows the reaction,  $x$ -, and  $y$ -diffusion term components of  $S_d^*$  for Case A at the same times as in Fig. 4. At the onset of the edge formation (Fig. 5(a)), it is clearly seen that the negative  $S_d^*$  observed in the leading part of the thermal thickness is primarily due to the negative value of the  $x$ -diffusion term,  $\partial/\partial x[\rho D_{H_2O}(\partial Y_{H_2O}/\partial x)]$ . At a later time (Fig. 5(b)), such effect disappears and  $S_d^*$  resumes a positive value throughout the thermal thickness. Since the  $x$ -diffusion term represents the enthalpy loss to the transverse direction (to the sides) of the edge, it is concluded that the negative edge flame speed is primarily caused by the edge structure whose thickness is highly squeezed by the excessive compressive strain rate in the presence of strong scalar dissipation rate.

The results shown in Figs. 4 and 5 thus suggest that a normal hydrogen-air edge flame is expected to assume a positive propagation speed through most of the lifetime, except during the very initial transient phase upon quenching. Nevertheless, accurate description of the transient edge dynamics can be essential in turbulent combustion modeling, since the turbulent eddies with such a large (near extinction) effective scalar dissipation rate are also likely to have a short characteristic time scale, in analogy with the scaling consideration as discussed in [20].

### ***Transient Dynamics***

To elaborate on the issues of transient dynamics and the large variation in  $S_d^*$  across the flame thickness,  $S_d^*$  as a function of  $\chi$  is plotted in Fig. 6, evaluated at various times and with various choices of  $Y_{H_2O}$  for Cases A to C. The speed is normalized by the laminar flame speed of the reference premixed flame,  $S_L^0$ . Each trajectory represents a temporal sequence of  $S_d^*$  and  $\chi$  at a given choice of  $Y_{H_2O}$ . As shown in Fig. 4, the displacement speed has a wide variation across the thermal thickness, which is clearly seen in Fig. 6 by the larger discrepancies among the four trajectories at earlier times. At later times, however, the sensitivity of  $S_d^*$  to the choice of  $Y_{H_2O}$  becomes very small, indicating that the strong initial transients have vanished.

The variations in the trajectories during the transient phase imply that the conventional  $S_d^*$  vs.  $\chi$  correlation is subjected to a large uncertainty depending on the definition of the edge location. As an attempt to reduce the uncertainty, it is recognized that the scalar dissipation rate is also affected by volume expansion across the flame as is the case with the displacement speed. Similar to the definition of  $S_d^*$ , we thus define the density-weighted scalar dissipation rate,  $\chi^* = \rho\chi / \rho_0$ , where  $\rho_0$  is the density of the mixture of the reference premixed flame at 1atm and 300K. Although  $S_d^*$  is a nondimensional variable,  $\chi^*$  is intentionally defined dimensional with a unit of  $s^{-1}$  due to the lack of proper characteristic time scale to normalize it. The results in Fig. 6 are then replotted in Fig. 7 in terms of  $S_d^*$  versus  $\chi^*$ , which show a remarkable collapse of the data for all cases. Therefore, it is suggested that  $\chi^*$  should be used as an appropriate parameter to characterize the propagation behavior of the edge flames with large thermal expansion, under both steady and transient conditions.

Although it is found that  $\chi^*$  can minimize the sensitivity of  $S_d^*$  to the details of the edge flame structure, it is not sufficient to explain the discrepancies among the correlations,  $S_d^*(\chi^*)$ , associated with the three different initial vortex conditions, as shown in Fig. 7. As the initial vortex strength increases, a higher edge flame speed can be achieved at an identical value of the instantaneous  $\chi^*$ . Furthermore, for stronger vortices (Cases B and C)  $S_d^*$  reaches a maximum value that is substantially larger than the reference laminar flame speed, suggesting that the edge flame response depends not only on the instantaneous value of  $\chi^*$ , but also on the detailed structure and history of the local flow after the edge formation.

The history effects on the detailed edge flame structures can be clearly seen by examining Fig. 2. Among the three cases studied, Case C generated an edge flame earlier than that the other cases due to the higher vortex strength, such that the strong vortices sustain for a longer period of time. Consequently, at a comparable  $\chi^*$  value, the detailed edge structure in Case C are substantially different from that in Case A, exhibiting a compressed front and broader lateral thickness, as shown in Fig. 2. This results in increased transport of fuel to generate additional heat release, and reduced transverse heat loss, hence leading to an increased displacement speed. It is of interest to note that, during the same period, the maximum heat release rate in Case C was found to be almost twice as large as that in Case A as well as that for the reference premixed flame, consistent with the relative difference in  $S_d^*$  between the two cases. The discrepancies in  $S_d^*$  among the three cases vanish asymptotically as  $\chi^*$  decreases, thereby ultimately approaching the laminar flame speed of the reference premixed flame. All these results suggest that, in realistic turbulent nonpremixed combustion, a universal correlation between  $S_d^*$  and  $\chi^*$

without considering the multi-dimensional, transient, and history effects may lead to significant errors for a substantial period of the edge lifetime.

### ***Effects of the Fuel Lewis Number***

To investigate the effect of Lewis number of fuel on the edge flame speed, two other cases, D and E, are simulated by artificially adjusting  $Le_{H_2}$  to 1.0 and 2.0, respectively (see Table 1). Since the diffusion flame strength and extinction limits are changed with the Lewis number, it is difficult to choose which of Cases A-C should be compared with. Considering the time of the edge formation and the detailed flame structure, Case C was found to be the most comparable condition and thus the results of  $S_d^*$  versus  $\chi^*$  for Cases C, D, and E are plotted in Fig. 8. Here  $S_d^*$  is normalized by the laminar flame speed of the reference premixed flame with the corresponding value of  $Le_{H_2}$ .

Three points stand out in Fig. 8. First, the existence of negative displacement speed is more prominent during the early stage of flame-vortex interaction as  $Le_{H_2}$  is increased. Therefore, the Lewis number effect predicted by Thatcher and Dold [7] based on steady edge flame propagation appears to be consistent under transient conditions. Secondly, an extremum in  $S_d^*$  also appears for larger Lewis number cases, suggesting that this behavior is rather attributed to the transient and history effects as discussed in Case C, than to the effect of the Lewis number. In other words, the presence of a peak in the curves in Figs. 7 and 8 must be distinguished from a similar nonmonotonic response in the edge flame speed observed in a steady analysis (for example, see Fig. 3 in Ref. [8]), which is only limited to smaller Lewis number cases. Lastly, the edge flame speed at small  $\chi^*$  values decreases as the fuel Lewis number increases. These values, however,

do not approach the freely-propagating laminar flame speed because the edge flame is subjected to a positive scalar dissipation rate imposed by the steady counterflow field. The behavior of the final edge flame speed (at approximately  $\chi^* = 200 \text{ s}^{-1}$ ) for various fuel Lewis number is also consistent with the theoretical prediction [7,8], in that  $S_d^*$  becomes lower as the fuel Lewis number increases due to the effect of the positive flame stretch.

In contrast to Fig. 7, the variation in the slope of the curves in Fig. 8 appears to suggest that the edge flame response becomes more sensitive to  $\chi^*$  as the fuel Lewis number is reduced. However, further investigation revealed that the Lewis number effect is not properly accounted for in characterizing in the scalar dissipation rate. Considering the flamelet equation for a reacting scalar  $\psi_i$  [3]:

$$\rho \frac{\partial \psi_i}{\partial t} = \frac{\rho \chi}{2\text{Le}_{\text{H}_2}} \frac{\partial^2 \psi_i}{\partial \xi^2} + \omega_i, \quad (3)$$

it is recognized that the appropriate effective scalar dissipation rate should be  $\chi_{\text{eff}}^* = \chi^* / \text{Le}_{\text{H}_2}$ . Figure 8 is then replotted for  $S_d^*$  versus  $\chi_{\text{eff}}^*$  in Fig. 9, which clearly shows that the slopes of the curves are comparable among the various fuel Lewis number cases. Therefore, the fuel Lewis number scaling based on the flamelet equation appears to be valid in describing the edge flame dynamics even considering the flow transients and detailed chemical species.

## Conclusion

Dynamics of edge flames generated by the quenching of counterflow nonpremixed flames has been studied via flame-vortex interactions. Unlike the edge flames that form by igniting fresh reactants, the edge flames arising from the nonpremixed flame quenching do not have a clearly

identifiable edge location immediately after the quenching. Edge flame speeds are thus found to vary significantly along the stoichiometric mixture fraction line within thermal thickness. It was found that the use of density-weighted displacement speed and scalar dissipation rate can effectively eliminate the ambiguity in determining the propagation speed of the edge flame with finite thickness and chemical structure, for both steady and transient conditions.

The three test cases with different vortex strengths demonstrated that the edge flame speed depends not only on the instantaneous local scalar dissipation rate, but also on the transient and history effects of the imposed flow field. A negative edge flame speed was observed only during the early phase of the interaction when the transient effect is large, primarily due to the enthalpy loss to the transverse direction in the presence of a large strain.

In constructing the submodels to describe partial quenching phenomena in turbulent nonpremixed combustion, the information during the early period of the edge flame behavior under near-extinction scalar dissipation rates is most critical. Therefore, a universal correlation between the displacement speed and the global scalar dissipation rate based entirely on steady counterflow models may lead to significant errors unless the transient and history aspects are carefully taken into account.

The dependence of the edge flame behavior on the fuel Lewis number were found to be overall consistent with previous theoretical predictions, showing a stronger prominence of the presence of negative flame speed at larger Lewis numbers. Consistent with the flamelet theory, the effective scalar dissipation rate scaled by the fuel Lewis number proved to be an appropriate parameter to characterize the edge flame with nonunity Lewis number under transient conditions.

## Acknowledgment

This work was supported by the Department of Energy, Office of Basic Energy Sciences, SciDAC Computational Chemistry Program.

## References

1. Dold, J. W., Hartley, L. J., and Green, D., in *Dynamical Issues in Combustion Theory* (P. C. Fife, A. Liñán, and F. A. Williams, eds.), IMA Volumes in Mathematics and Its Applications, 35, Springer-Verlag, New York, 1991, pp. 83-105.
2. Buckmaster, J. and Zhang, Y., *Combust. Theory Modelling* 2 (1998) 449-177.
3. Peters, N., *Turbulent Combustion*, Cambridge (2000).
4. Hasselbrink, E. F. and Mungal, M. G., *Proc. Combust. Inst.*, 27 (1998) 867-873.
5. Ko, Y. S. and Chung, S. H., *Combust. Flame* 118 (1-2) (1999) 151-163.
6. Vedarjan, T. G., Buckmaster, J., and Ronney, P., *Proc. Combust. Inst.* 27 (1998) 537-544.
7. Thatcher, R. W. and Dold, J. W., *Combust. Theory Modelling* 4 (2000) 435-457.
8. Daou, J. and Liñán, A., *Combust. Theory Modelling* 2 (1998) 449-477.
9. Daou, R., Daou, J., and Dold, J., *Proc. Combust. Inst.* 29 (2002) 1559-1564.
10. Favier, V. and Vervisch, L., *Combust. Flame* 125 (1-2) (2001) 788-803.
11. Boulanger J. and Vervisch, L., *Combust. Flame* 130 (1-2) (2002) 1-14.
12. Lee, J., Frouzakis, C. E., and Boulouchos, K., *Proc. Combust. Inst.* 28 (2000) 801-806.
13. Frouzakis, C. E., Tomboulides, A. G., Lee, J., and Boulouchos, K., *Proc. Combust. Inst.* 29 (2002) 1581-1587.
14. Echehki and Chen, J. H., *Combust. Flame* 114 (1-2) (1998) 231-245.
15. Im, H. G. and Chen, J. H., *Combust. Flame* 119 (4) (1999) 436-454.

16. Im, H. G. and Chen, J. H., *Combust. Flame* 126 (1-2) (2001)1384-1392.
17. Mueller, M. A., Yetter, R. A., and Dryer, F. L., *Proc. Combust. Inst.* 27 (1998) 117-184.
18. Yoo, C. S. and Im, H. G., *Proc. 3<sup>rd</sup> Joint Meeting of U.S. Sections of the Combust. Inst.* (2003).
19. Bilger, R. W., *Proc. Combust. Inst.* 22 (1988) 475-488.
20. Im, H. G., Bechtold, J. K., and Law, C. K., *Combust. Sci. Tech.* 106 (1995) 345-361.

Parameter	case A	case B	case C	case D	case E
$u_{\theta, \max}$ [cm/s]	3700	4500	6000	3500	3500
$u_0$ [cm/s]	940	940	940	500	500
$u_L$ [cm/s]	710	710	710	350	350
$\sigma$ [mm]	0.50	0.50	0.50	0.50	0.50
$\delta$ [mm]	0.80	0.80	0.80	0.80	0.80
$\rho_1$ [cm]	0.12	0.12	0.12	0.12	0.12
$\rho_2$ [cm]	0.344	0.344	0.344	0.365	0.365
$Le_{H_2}$	0.32	0.32	0.32	1.0	2.0

**Table 1**

Physical parameters used in the study. See Eq. (1) and Fig. 1 for the definition of various parameters.

## List of Figure Captions

- Fig. 1 Computational configuration of the flame-vortex interaction. The solid and dashed contour lines denote vorticity magnitude and  $x$ -directional velocity, respectively.
- Fig. 2 Temporal evolution of the heat release isocontours for Cases A-C. Dashed line represents the stoichiometric mixture fraction line ( $\mathcal{Z}^*$  is measured at  $Y_{\text{H}_2\text{O}} = 0.04$ ).
- Fig. 3 Evolution of the heat release rate profile in  $y$ -direction along the stoichiometric mixture fraction line for Case A.
- Fig. 4 The displacement speed, mass fraction of  $\text{H}_2\text{O}$ , and normalized heat release rate along the stoichiometric mixture fraction line at (a)  $t = 0.265\text{ms}$  and (b)  $t = 0.367\text{ms}$  for Case A. Note that the displacement speed is meaningful only within thermal thickness as denoted by the shaded area.
- Fig. 5 The diffusion and reaction rate effects on the displacement speed at (a)  $t = 0.265\text{ms}$  and (b)  $t = 0.367\text{ms}$  for Case A.
- Fig. 6 The density-weighted displacement speed as a function the scalar dissipation rate for  $Y_{\text{H}_2\text{O}} = 0.03, 0.035, 0.04, 0.045$  for Cases A to C.
- Fig. 7 The density-weighted displacement speed as a function of the density-weighted scalar dissipation rate for  $Y_{\text{H}_2\text{O}} = 0.03, 0.035, 0.04, 0.045$  for Cases A to C.
- Fig. 8 The density weighted displacement speed with the density-weighted scalar dissipation rate for  $Y_{\text{H}_2\text{O}} = 0.03\text{--}0.045$  for Cases C, D, and E.
- Fig. 9 The density weighted displacement speed with the effective density-weighted scalar dissipation rate for  $Y_{\text{H}_2\text{O}} = 0.03\text{--}0.045$  for Cases C, D, and E.

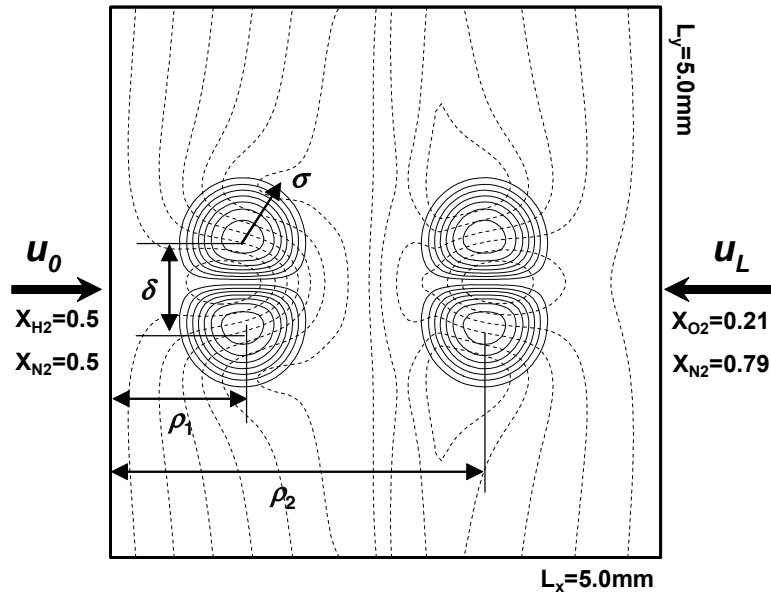


Fig 1. Computational configuration of the flame-vortex interaction. The solid and dashed contour lines denote vorticity magnitude and  $x$ -directional velocity, respectively.

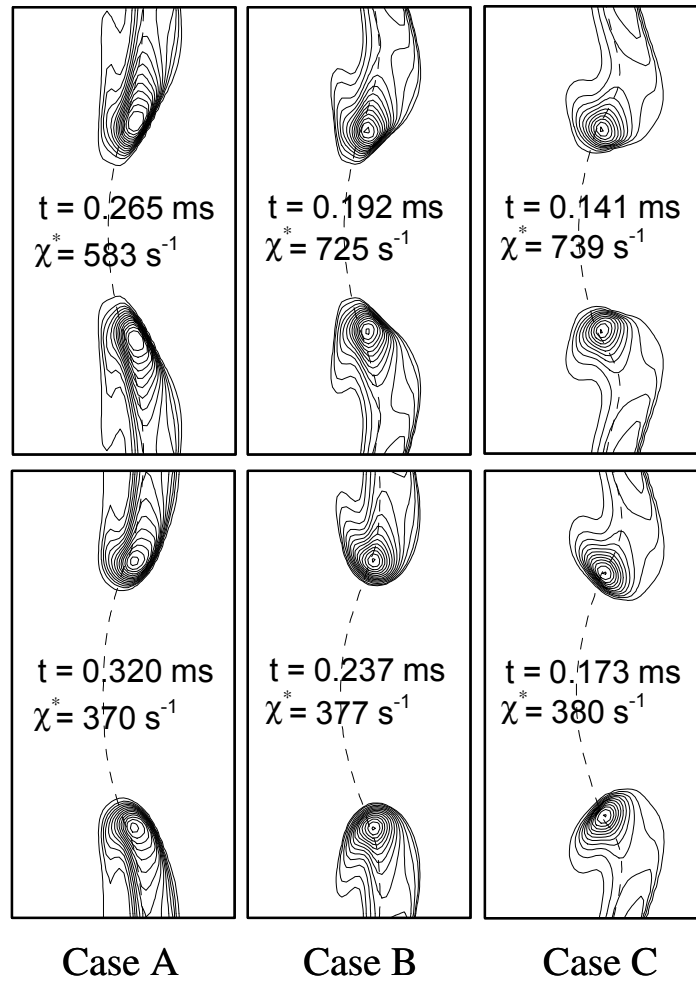


Fig 2. Temporal evolution of the heat release isocontours for Cases A-C. Dashed line represents the stoichiometric mixture fraction line ( $\chi^*$  is measured at  $Y_{H_2O} = 0.04$ ).

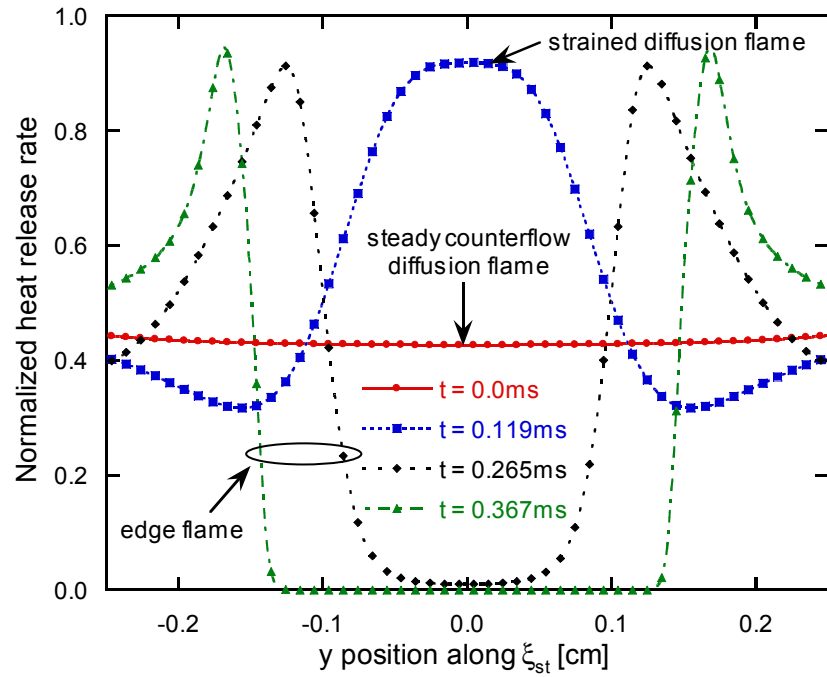


Fig. 3 Evolution of the heat release rate profile in y-direction along the stoichiometric mixture fraction line for Case A.

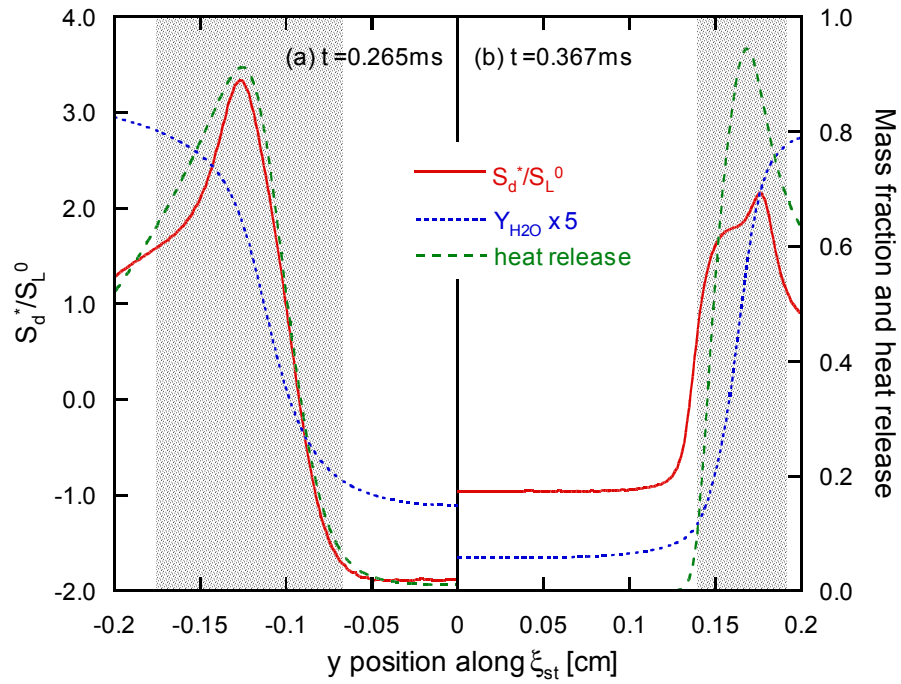


Fig. 4 The displacement speed, mass fraction of  $\text{H}_2\text{O}$ , and normalized heat release rate along the stoichiometric mixture fraction line at (a)  $t = 0.265\text{ms}$  and (b)  $t = 0.367\text{ms}$  for Case A. Note that the displacement speed is meaningful only within thermal thickness as denoted by the shaded area.

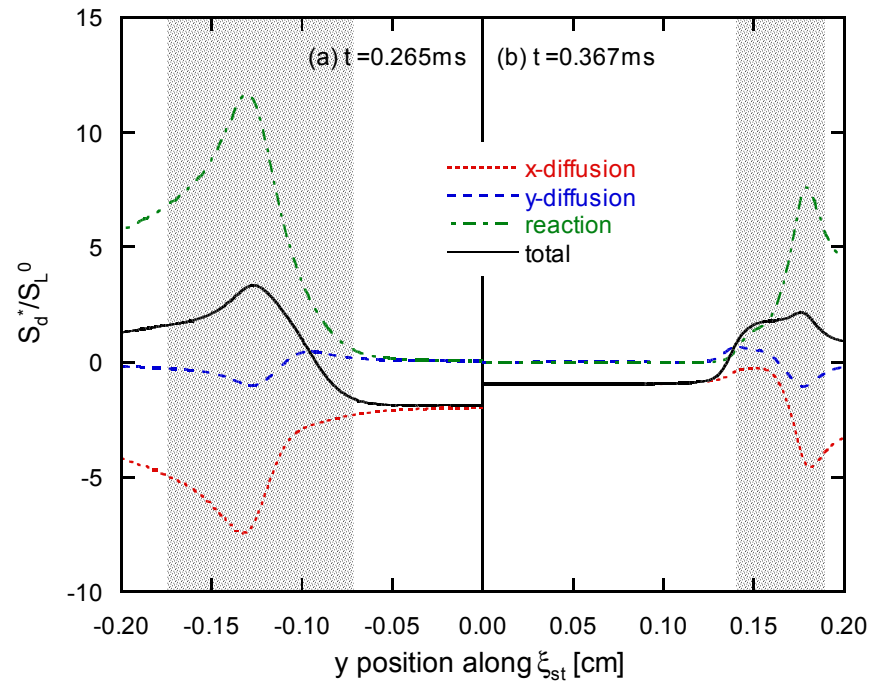


Fig. 5 The diffusion and reaction rate effects on the displacement speed at (a)  $t = 0.265$ ms and (b)  $t = 0.367$ ms for Case A.

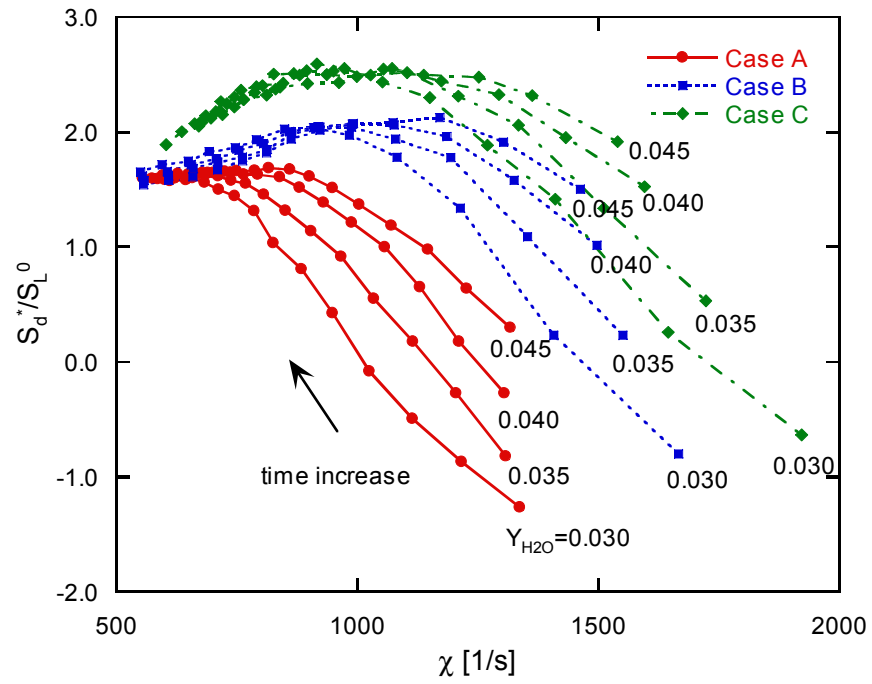


Fig. 6 The density-weighted displacement speed as a function the scalar dissipation rate for  $Y_{\text{H}_2\text{O}} = 0.03, 0.035, 0.04, 0.045$  for Cases A to C.

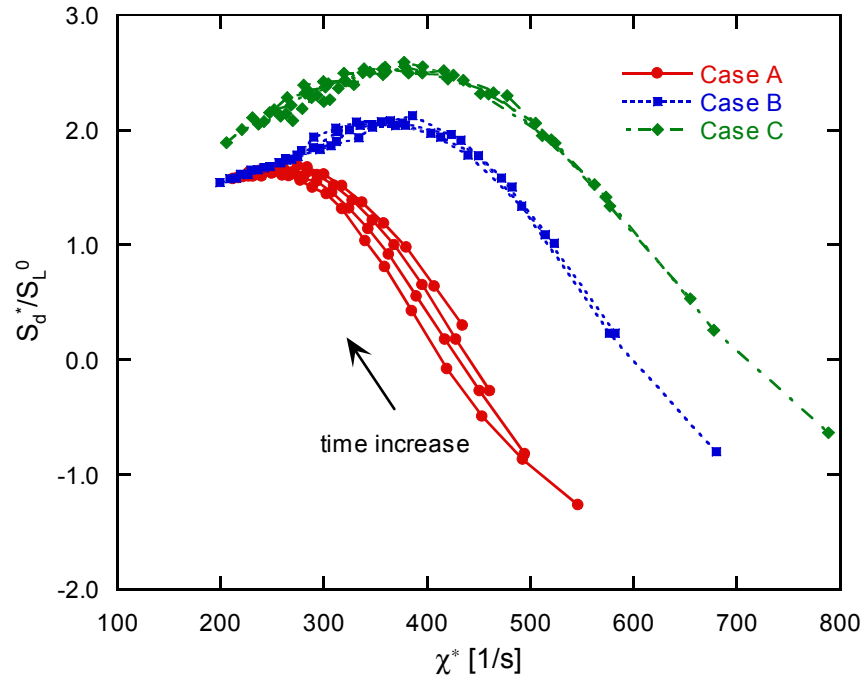


Fig. 7 The density-weighted displacement speed as a function of the density-weighted scalar dissipation rate for  $Y_{\text{H}_2\text{O}} = 0.03, 0.035, 0.04, 0.045$  for Cases A to C.

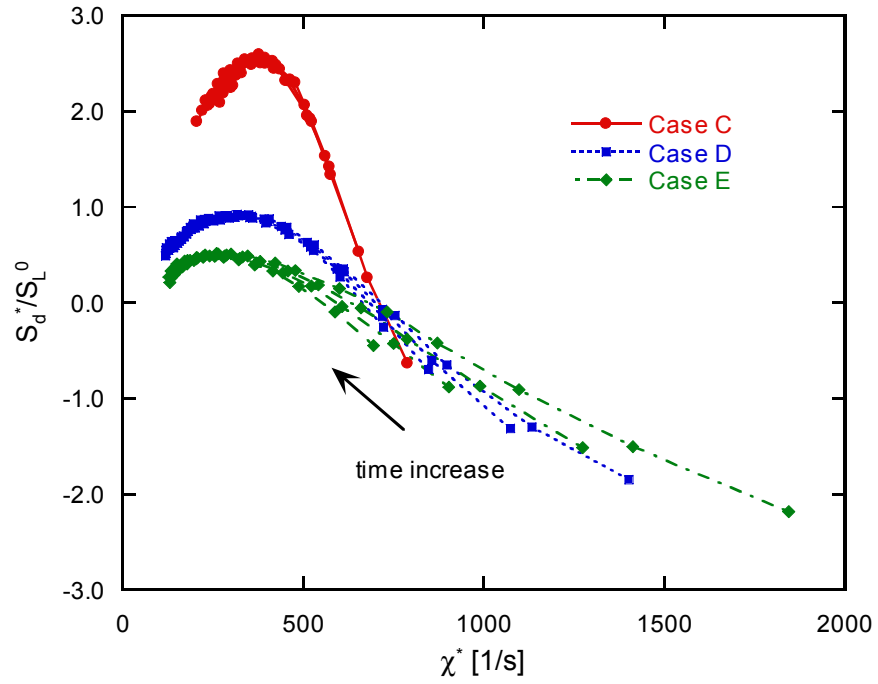


Fig. 8 The density weighted displacement speed with the density-weighted scalar dissipation rate for  $Y_{H_2O} = 0.03-0.045$  for Cases C, D, and E.

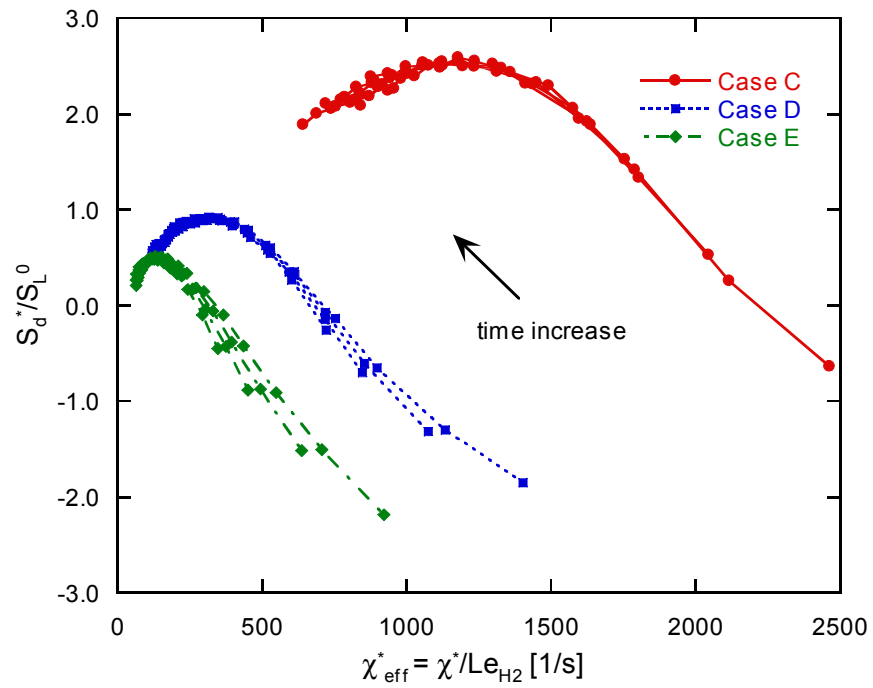


Fig. 9 The density weighted displacement speed with the effective density-weighted scalar dissipation rate for  $Y_{\text{H}_2\text{O}} = 0.03\text{--}0.045$  for Cases C, D, and E.